

# Off-Shell Structures of Nucleon-Nucleon t-matrices and their Influence on Nucleon-Nucleus Elastic Scattering Observables

S.P. Weppner

*Natural Arts and Sciences, Eckerd College, St. Petersburg, FL 33711*

Ch. Elster

*Institute of Nuclear and Particle Physics, and Department of Physics and Astronomy,  
Ohio University, Athens, OH 45701*

D. Hüber

*Theoretical Division, Los Alamos National Laboratory, Los Alamos NM, 87545*  
(October 24, 2018)

## Abstract

The sensitivity of nucleon-nucleus elastic scattering observables to the off-shell structure of nucleon-nucleon t-matrices, derived from realistic NN potentials, is investigated within the context of a full-folding model based on the impulse approximation. Our study uses recently developed NN potential models, which describe a subset of the NN data base with a  $\chi^2$  per datum  $\sim 1$ , which means that the NN t-matrices are essentially on-shell equivalent. We calculate proton-nucleus elastic scattering observables for  $^{16}\text{O}$ ,  $^{40}\text{Ca}$ , and  $^{208}\text{Pb}$  between 100 and 200 MeV laboratory energy. We find that the elastic scattering observables are insensitive to off-shell differences of the employed NN t-matrices. A more detailed investigation of the scattering equation and the optical potential as given in a factorized approximation reveals that the elastic scattering observables do not sample the NN t-matrices very far off-shell where they exhibit differences.

PACS: 25.40.Cm, 24.10-Ht

Typeset using REVTeX

## I. INTRODUCTION

Theoretical investigations of nucleon-nucleon (NN) transition amplitudes in their off-shell domain have a long history in the study of few and many-nucleon systems. Often those investigations were inconclusive due to the lack of NN potentials which describe the NN observables with equally high accuracy. Current interest in this issue is driven by the recent development of NN potentials which below pion production threshold describe the NN data base with a  $\chi^2$  per datum  $\sim 1$  [1–3]. Transition amplitudes derived from these potentials can be considered on-shell equivalent. Their different theoretical derivation gives rise to different off-shell extrapolations.

At intermediate energies elastic nucleon-nucleus (NA) scattering can be successfully described by the leading term in the spectator expansion of multiple scattering theory [4–6]. Here an optical potential is derived, which in its most general form is given by the expectation value of the NN transition amplitude and the ground state of the target nucleus. This ‘full-folding’ optical potential involves the convolution of the fully off-shell NN scattering amplitude with a realistic single particle nuclear density matrix.

Recently, significant advances have been made in accurately handling these off-shell degrees of freedom in elastic NA scattering [7–11]. Those studies have demonstrated that an accurate treatment of the off-shell structure of the NN transition amplitude is needed for a proper account of the theory. In order to cleanly isolate if NA elastic scattering observables are sensitive to different off-shell structures of realistic NN transition amplitudes, it is necessary to start from NN potentials which describe the NN data base with a high degree of accuracy. Our present study is based on the potential models for the NN interaction recently developed by the Nijmegen group [1] and the charge-dependent Bonn (CD-Bonn) potential [2]. With NN transition amplitudes derived from these potentials we calculate full-folding optical potentials and elastic scattering observables for proton scattering from a variety of nuclei in the energy regime between 100 and 200 MeV projectile energy. Although the off-shell structure of the NN t-matrices is an important ingredient in the calculations, we find that off-shell differences between the models are not discernible by NA elastic scattering.

In order to understand this result and obtain more insight which regions of the off-shell NN t-matrix are sampled in a calculation of NA elastic scattering observables, we use the optimum factorized or off-shell  $t\rho$  formulation of the optical potential. This formulation, quite a good approximation in the energy regime around 200 MeV and higher, has the advantage that the fully off-shell NN t-matrix enters together with an on-shell density.

The structure of this article is as follows. First we review in Section II the relevant expressions for the full-folding optical potential as used in our calculations. In Section III we present elastic scattering results for proton scattering from a variety on nuclei based on the Nijmegen and CD-Bonn potentials. In Section IV we present a detailed study on which off-shell regions of the NN t-matrix are sampled in a calculation of the elastic scattering observables. This study is based on the factorized  $t\rho$  approximation to the full-folding optical potential and is carried out at 200 MeV projectile energy. We end with concluding remarks in Section V.

## II. THEORETICAL FRAMEWORK FOR THE OPTICAL POTENTIAL

The transition amplitude for elastic scattering of a projectile from a target nucleus is given as [6]

$$T_{el} = PUP + PUG_0(E)T_{el}, \quad (2.1)$$

where  $P$  is the projector on the ground state  $|\Phi_A\rangle$  of the target,  $P = \frac{|\Phi_A\rangle\langle\Phi_A|}{\langle\Phi_A|\Phi_A\rangle}$ ,  $G_0(E) = (E - H_0 + i\varepsilon)^{-1}$ , and  $U$  represents the optical potential. For the scattering of a single particle projectile from an A-particle target nucleus the free Hamiltonian is given by  $H_0 = h_0 + H_A$ , where  $h_0$  is the kinetic energy operator for the projectile and  $H_A$  stands for the target Hamiltonian. In the spirit of the spectator expansion the target Hamiltonian is viewed as  $H_A = h_i + \sum_{j \neq i} v_{ij} + H^i$ , where  $h_i$  is the kinetic energy operator for the  $i$ th target nucleon,  $v_{ij}$  the interaction between target nucleon  $i$  and the other target nucleons  $j$ , and  $H^i$  is an (A-1)-body operator containing all higher order effects. In a mean field approximation  $\sum_{j \neq i} v_{ij} \approx W_i$ , where  $W_i$  is assumed to depend only on the  $i$ th particle coordinate. In this present work we want to concentrate only on the impulse approximation, which is a good approximation in the intermediate energy regime (around 200 MeV projectile energy and higher), where the influence of  $W_i$  can be neglected [6]. Thus the propagator  $G_0(E)$  in the impulse approximation is given as

$$G_0(E) \approx g_i(E) = [(E - E^i) - h_0 - h_i + i\varepsilon]^{-1}. \quad (2.2)$$

Here  $H^i$ , having no explicit dependence on the  $i$ th particle, is replaced by an average energy  $E^i$ . In the present calculations we set  $E_i = 0$ . In the energy regime considered in this work, the effect of a value of  $E_i$  of the order of the separation energy of a nucleon from a nucleus is negligible [11,12].

The driving term of Eq. (2.1) denotes the optical potential, which in first order is given as

$$\langle \mathbf{k}' | \langle \Phi_A | PUP | \Phi_A \rangle | \mathbf{k} \rangle \equiv \hat{U}(\mathbf{k}', \mathbf{k}) = \sum_{i=n,p} \langle \mathbf{k}' | \langle \Phi_A | \hat{\tau}_{0i}(\mathcal{E}) | \Phi_A \rangle | \mathbf{k} \rangle. \quad (2.3)$$

Here  $\mathbf{k}'$  and  $\mathbf{k}$  are the external momenta of the system,  $\hat{\tau}_{0i}(\mathcal{E})$  represents the NN transition operator

$$\hat{\tau}_{0i}(E) = v_{0i} + v_{0i}g_i(E)\hat{\tau}_{0i}(E), \quad (2.4)$$

with  $g_i(E)$  given in Eq. (2.2) and  $v_{0i}$  representing the NN interaction. The sum over  $i$  in Eq. (2.3) indicates the two different cases, namely when the target nucleon is one of  $Z$  protons, and when it is one of  $N$  neutrons. The energy  $\mathcal{E}$  is the relative energy of the interacting two-nucleon system. Inserting a complete set of momenta for the struck target nucleon before and after the collision and evaluating the momentum conserving  $\delta$ -functions gives as final expression for the full-folding optical potential [10,12]

$$\hat{U}(\mathbf{q}, \mathbf{K}) = \sum_{i=n,p} \int d^3P \eta(\mathbf{P}, \mathbf{q}, \mathbf{K}) \hat{\tau}_{0i}(\mathbf{q}, \frac{1}{2}(\frac{A+1}{A}\mathbf{K} - \mathbf{P}), \mathcal{E}) \rho_i(\mathbf{P} - \frac{A-1}{A}\frac{\mathbf{q}}{2}, \mathbf{P} + \frac{A-1}{A}\frac{\mathbf{q}}{2}). \quad (2.5)$$

Here the arguments of the NN amplitude  $\hat{\tau}_{0i}$  are  $\mathbf{q} = \mathbf{k}' - \mathbf{k} = \mathbf{k}_{\text{NN}'} - \mathbf{k}_{\text{NN}}$  and  $\frac{1}{2}(\mathbf{k}_{\text{NN}'} + \mathbf{k}_{\text{NN}}) = \frac{1}{2}(\frac{A+1}{A}\mathbf{K} - \mathbf{P})$ , where

$$\mathbf{k}'_{\text{NN}} = \frac{1}{2}(\mathbf{k}' - (\mathbf{P} - \frac{\mathbf{q}}{2} - \frac{\mathbf{K}}{A})) \quad (2.6)$$

and

$$\mathbf{k}_{\text{NN}} = \frac{1}{2}(\mathbf{k} - (\mathbf{P} + \frac{\mathbf{q}}{2} - \frac{\mathbf{K}}{A})) \quad (2.7)$$

are the nonrelativistic final and initial nuclear momentum in the zero momentum frame of the NN system, and  $\mathbf{K} = \frac{1}{2}(\mathbf{k}' + \mathbf{k})$ . The factor  $\eta(\mathbf{P}, \mathbf{q}, \mathbf{K})$  is the Møller factor for the frame transformation [13], and  $\rho_i$  represents the density matrix of the target for either protons or neutrons. Evaluating the propagator  $g_i(E)$  of Eq. (2.2) in the nucleon-nucleus (NA) center of mass frame yields for the energy argument  $\mathcal{E}$  of the NN amplitude  $\hat{\tau}_{0i}$  of Eq. (2.5)

$$\mathcal{E} = E_{\text{NA}} - \frac{(\frac{A-1}{A}\mathbf{K} + \mathbf{P})^2}{4m_N}. \quad (2.8)$$

Here  $E_{\text{NA}}$  is the total energy in the NA center of mass frame and  $m_N$  is the nucleon mass.

The expression for the optical potential as given in Eq. (2.5) shows that the evaluation of the full-folding integral requires the NN t-matrix fully off-shell as well as at positive energies from  $E_{\text{NA}}$  to negative energies [7,8,11].

### III. PROTON ELASTIC SCATTERING OBSERVABLES

In this paper the study of elastic scattering of protons from spin zero target nuclei at energies between 100 and 200 MeV incident projectile energy is strictly first order based on the impulse approximation. The full-folding optical potentials are calculated according to Eq. (2.5). The details of the calculations are given in Refs. [10,11]. As a model for the density matrix for the target nucleus we employ a Dirac-Hartree (DH) calculation [14]. The Fourier transform of the vector density,  $\rho(\mathbf{r}', \mathbf{r})$ , serves as our non-relativistic single particle density [10]. The crucial ingredient under investigation here is the fully off-shell NN t-matrix. The calculations presented here employ NN t-matrices based on two different potentials given by the Nijmegen group [1] and the charge-dependent Bonn potential [2]. All three potentials are fitted to describe the Nijmegen data base with a  $\chi^2$  per datum  $\sim 1$ . An essential difference between the two Nijmegen models is the presence of a momentum dependent, nonlocal term in the central piece of the NijmI potential, whereas the NijmII model is strictly local. Both Nijmegen potentials have a  $\chi^2$  per datum = 1.03 with respect to both, the neutron-proton and the proton-proton data base. The CD-Bonn potential is nonlocal due to the structure of the relativistic meson-nucleon vertices. An additional nonlocality is contained due to the so-called minimal relativity factors  $\sqrt{m/E}$ , which are necessary to maintain the relativistic unitarity condition. The CD-Bonn potential also describes the Nijmegen data base with a  $\chi^2$  per datum = 1.03. All three potential models describe the Nijmegen data base with the same high degree of accuracy, thus the NN t-matrices can be considered on-shell equivalent. From their different theoretical derivation it can be expected that they have different extrapolations off-shell.

When calculating  $\hat{U}(\mathbf{q}, \mathbf{K})$  as given in Eq. (2.5), it is to be understood that all spin summations are carried out. This reduces the required NN t-matrix elements to a spin independent component (corresponding to the Wolfenstein amplitude A) and a spin-orbit component (corresponding to the Wolfenstein amplitude C). Since we are assuming that we have spin saturated nuclei, the components of the NN t-matrix depending on the spin of the struck target nucleon vanish. The Coulomb interaction between the projectile and the target is included using the exact formulation of Ref. [15].

At first we want to concentrate on proton scattering from different target nuclei at 200 MeV projectile energy. In Fig. 1 we display the differential cross section  $d\sigma/d\Omega$ , the analyzing power  $A_y$ , and the spin rotation function  $Q$  for elastic proton scattering from  $^{16}\text{O}$ . The solid line represents a calculation based employing the CD-Bonn t-matrix as input, the dashed line is based on the one derived from the NijmI potential and the dash-dotted line the one derived from the NijmII model. All three calculations are remarkably close to each other, and all three fail to describe the dips in the analyzing power. The same statement is true for proton scattering from  $^{40}\text{Ca}$  at 200 MeV, which is displayed in Fig. 2. In Fig. 3 we show the elastic scattering observables for proton scattering from  $^{208}\text{Pb}$  at 200 MeV. Again, all three NN potential models give nearly identical results, however the spin observables are described slightly better for  $^{208}\text{Pb}$ .

At lower energies the scattering observables may exhibit a somewhat larger sensitivity to the energy dependence of the NN t-matrix due to the closer proximity of the deuteron pole and the virtual  $^1\text{S}_0$  state. In order to study the sensitivity of the NA scattering observables to different NN t-matrices at lower energies we show in Fig. 4 the observables for proton scattering from  $^{40}\text{Ca}$  at 160 MeV and in Fig. 5 the ones for proton scattering from  $^{16}\text{O}$  at 135 MeV. Again, all three potential models lead to nearly identical results.

We do not want to carry out further studies at lower energies, since it is well known that the impulse approximation alone is not adequate to describe the scattering observables at lower energies [6,7,11]. We prefer to pursue further investigations to find out why expected off-shell differences in the potential models are not visible in the elastic NA observables.

#### IV. INVESTIGATION OF OFF-SHELL DIFFERENCES

In the full-folding optical potential as given in Eq. (2.5) the energy of propagation in the NN t-matrix is coupled to the integration variable. This makes it difficult to access effects resulting from the off-shell structure of the NN t-matrices separately. For this reason, we prefer to carry out the following study using the optimum factorized form of the optical potential, which has been shown to be quite a good approximation to the full-folding expression at projectile energies of 200 MeV and higher [11]. The optimum factorized form is characterized by two approximations. First, the energy  $\mathcal{E}$  of the NN t-matrix in Eq. (2.5) is fixed at half the projectile energy (in the laboratory frame)

$$\mathcal{E} \equiv E_0 = \frac{1}{2} \frac{k_{lab}^2}{2m_N} = \frac{1}{2} \frac{\left(\frac{A+1}{A} k_0\right)^2}{2m_N}. \quad (4.1)$$

Here  $k_{lab}$  and  $k_0$  are the on-shell momenta in the laboratory and NA system respectively, and  $m_N$  is the mass of a nucleon. Second, the NN t-matrix and the Møller factor are expanded

in  $\mathbf{P}$  around a fixed value  $\mathbf{P}_0$ , determined by the requirement that the contribution of the first derivative term is minimized. For elastic scattering the contribution vanishes if  $\mathbf{P}_0$  is chosen to be zero [16,17]. With these assumptions, the expression for the optical potential in the optimum factorized form is given as

$$\hat{U}_{fac}(\mathbf{q}, \mathbf{K}) = \sum_{i=p,n} \eta(\mathbf{q}, \mathbf{K}) \hat{\tau}_{0i} \left( \mathbf{q}, \frac{A+1}{2A} \mathbf{K}, E_0 \right) \rho_i(q). \quad (4.2)$$

In this form the non-local character of the optical potential is solely determined by the off-shell NN t-matrix and the Møller factor. If we now consider the integral equation for elastic NA scattering as given in Eq. (2.1), we see that only the second term in the right hand side of Eq. (2.1) contains the integration over the optical potential. The driving term,  $\hat{U}_{fac}(\mathbf{k}'_0, \mathbf{k}_0, E)$  contains the NN t-matrix evaluated at the fixed momenta  $\mathbf{k}'_0$  and  $\mathbf{k}_0$ , multiplied with the density profile  $\rho_i(q)$ . In this case the momentum vectors  $\mathbf{q}$  and  $\mathbf{K}$  are  $\mathbf{q} = \mathbf{k}'_0 - \mathbf{k}_0$  and  $\mathbf{K} = \frac{1}{2}(\mathbf{k}'_0 + \mathbf{k}_0)$ .

In order to study off-shell effects, we define the following quantity

$$B(\mathbf{k}'_0, \mathbf{k}_0, E) = \lim_{\epsilon \rightarrow 0} \int_0^\infty d^3\mathbf{k}'' \frac{\hat{U}_{fac}(\mathbf{k}'_0, \mathbf{k}'', E) T(\mathbf{k}'', \mathbf{k}_0, E)}{E - E(k'') + i\epsilon}, \quad (4.3)$$

where  $T(\mathbf{k}'', \mathbf{k}_0, E)$  is the solution of Eq. (2.1), obtained using the optical potential in the factorized form. Here  $B(\mathbf{k}'_0, \mathbf{k}_0, E)$  represents the integral on the right-hand side of Eq. (2.1), and thus the quantity in which the optical potential  $U$  enters off-shell when calculating  $T_{el}$ . Since the nuclear density in momentum space is a function strongly peaked for small momenta, we may conjecture that the density will dominate the fall-off behavior of  $\hat{U}_{fac}(\mathbf{k}'_0, \mathbf{k}'', E)$  for large values of the integration variable  $\mathbf{k}''$ . To investigate this more closely, we write Eq. (4.3) as

$$B(\mathbf{k}'_0, \mathbf{k}_0, E) = \lim_{\epsilon \rightarrow 0} \int d\Omega'' \int_0^{k_{max}} dk'' k''^2 \frac{\hat{U}_{fac}(\mathbf{k}'_0, \mathbf{k}'', E) T(\mathbf{k}'', \mathbf{k}_0, E)}{E - E(k'') + i\epsilon}, \quad (4.4)$$

and study the behavior of  $B(\mathbf{k}'_0, \mathbf{k}_0, E)$  as a function of  $k_{max}$ . Since  $B(\mathbf{k}'_0, \mathbf{k}_0, E)$  depends on vector variables, we actually have  $B(k_0, k_0, \theta, E)$ , where  $\theta$  is the angle between  $\mathbf{k}'_0$  and  $\mathbf{k}_0$ . In Fig. 6 we show the real part  $Re B(k_0, k_0, \theta, E)$  for different values of  $k_{max}$  for neutron scattering from  $^{16}\text{O}$  at 200 MeV projectile energy, and in Fig. 7 for neutron scattering from  $^{90}\text{Zr}$  at the same energy. We see that in the case of  $^{16}\text{O}$  an integration up to  $k_{max} = k_0 + 1.0 \text{ fm}^{-1}$  is already sufficient to obtain the full result. In the case of  $^{90}\text{Zr}$  one only needs to integrate to  $k_{max} = k_0 + 0.5 \text{ fm}^{-1}$  to have a result identical to the complete integral. In both cases  $k_0 \sim 3 \text{ fm}^{-1}$ . When considering the imaginary part of  $B(k_0, k_0, \theta, E)$  we arrive at the same conclusion. We carried out similar tests at different energies and arrived essentially at the same values for  $k_{max}$  for the two different nuclei. Assuming that the nuclear density is responsible for the fast fall-off of the optical potential as function of  $\mathbf{k}'$ , this finding is not surprising. From Figs. 6 and 7 we also see that for a heavier nucleus the contribution beyond the on-shell value  $k_0$  is much less than for a light nucleus. Again, this is not too surprising, when one recalls the functional form of the nuclear density profiles. The density profile  $\rho_p(q)$  for the proton distribution of  $^{16}\text{O}$  has its first minimum at  $q \sim 2 \text{ fm}^{-1}$ , whereas the proton distribution of  $^{90}\text{Zr}$  has its first minimum at  $q \sim 1 \text{ fm}^{-1}$ .

In order to verify that the functional form of the density is the limiting factor for the range of the integration, we identify in Eq. (4.4)  $T(\mathbf{k}'', \mathbf{k}_0, E)$  as well as  $\hat{U}_{fac}(\mathbf{k}_0, \mathbf{k}'', E)$  with the density  $\rho(|\mathbf{k}'' - \mathbf{k}_0|) = \sum_{i=p,n} \rho_i(|\mathbf{k}'' - \mathbf{k}_0|)$  to obtain

$$B'(\mathbf{k}'_0, \mathbf{k}_0, E) = \lim_{\epsilon \rightarrow 0} \int d\Omega'' \int_0^{k_{max}} dk'' k''^2 \frac{\rho(|\mathbf{k}'' - \mathbf{k}_0|)\rho(|\mathbf{k}'' - \mathbf{k}'_0|)}{E - E(k'') + i\epsilon}, \quad (4.5)$$

and repeat the above study, namely consider  $B'(k_0, k_0, \theta, E)$  as a function of  $k_{max}$ . In Fig. 8 we plot the real part  $Re B'(k_0, k_0, \theta, E)$  using different integration ranges. The result is similar to the one in Fig. 6 and 7. Considering Fig. 8 the upper bound for the integral can be constrained to  $k_0 + 1.5 \text{ fm}^{-1}$ . Since the integral in Eq. (4.5) is symmetric about the on-shell value, the lower bound of integration can be constrained to  $k_0 - 1.5 \text{ fm}^{-1}$ .

After having found that only a limited region of the NN t-matrix enters a calculation of NA elastic scattering observables, we need to project this region, namely  $k_0 \pm 1.5 \text{ fm}^{-1}$ , on the NN t-matrices and see if the t-matrices employed in our calculations differ in this restricted region. Thus we show first in Fig. 9 the real part of the off-shell Wolfenstein amplitude  $A$ ,  $Re A(k'_{NN}, k_{NN}, E_0)$ , at 200 MeV obtained from the NijmI potential as function of  $k_{NN}$  and  $k'_{NN}$ . Here the angle between  $\mathbf{k}_{NN}$  and  $\mathbf{k}'_{NN}$  is chosen to be zero. The value of the on-shell momentum is located at  $k_{NN} = k'_{NN} = 1.55 \text{ fm}^{-1}$ . It should be noted that the values of  $Re A$  in the plotted domain range between 0.6 and -3  $\text{MeVfm}^3$ . Since the study of the integration bounds in the integral  $B(k_0, k_0, \theta, E)$  was carried out using momenta defined in the NA system, we use Eqs. (2.6) and (2.7) to transform the bounds to momenta given in the NN system. As a reminder, since we work in the optimum factorized form, the momentum  $\mathbf{P}$  in Eqs. (2.6) and (2.7) is zero. Using these transformations, which are explicitly given as  $\mathbf{k}'_{NN} = \frac{1}{4}[(1/A + 3)\mathbf{k}'_0 + (1/A - 1)\mathbf{k}'']$  and  $\mathbf{k}_{NN} = \frac{1}{4}[(1/A - 1)\mathbf{k}'_0 + (1/A + 3)\mathbf{k}'']$ , we obtain the ‘skew box’ given in Fig. 9 as region of the NN t-matrix whose values enter the NA scattering equation.

Next, we display in Fig. 10 the difference between the real parts of the Wolfenstein amplitudes  $Re A(k'_{NN}, k_{NN}, E_0)$  given by the NijmI and CD-Bonn potentials, again as function of  $k_{NN}$ ,  $k'_{NN}$  and the angle between the two vectors being zero. First we notice that within the plotted region the off-shell differences between the two amplitudes is relatively small. Only for  $k_{NN} = k'_{NN} \sim 5 \text{ fm}^{-1}$  there is a difference larger than  $0.2 \text{ MeVfm}^3$ . Again, the on-shell value is located at  $k_{NN} = k'_{NN} = 1.55 \text{ fm}^{-1}$ . The region which enters a calculation of NA scattering observables is again indicated by a ‘skew box’. Within this box there are essentially no differences between the amplitudes. The largest difference is located in the upper right corner of the ‘skew box’ almost opposite the on-shell point, and is about 6% of the total value of  $Re A$ .

In Fig. 11 we show the difference between the real parts of the Wolfenstein amplitudes derived from the NijmI and NijmII potentials. These two amplitudes show off-shell differences of  $1 \text{ MeVfm}^3$  and larger for values of  $k_{NN} = k'_{NN} \sim 4 \text{ fm}^{-1}$ . However, in the region which is sampled by NA scattering calculations (‘skew box’) both amplitudes are nearly identical in the lower left half around the on-shell value. Larger differences between those two potentials are located in the upper right corner furthest away from the on-shell value. For the other Wolfenstein amplitude, which enters our calculations of elastic NA scattering observables, we obtain similar conclusions. A close inspection of the scattering observables for the light nuclei  $^{16}\text{O}$  and  $^{40}\text{Ca}$  in Figs. 1 and 2 shows that the dash-dotted

curves representing the calculations with the NijmII model can be distinguished from the other two curves, especially at larger angles. However, the differences in the observables are still quite small, indicating the calculations are dominated by the area around the on-shell value.

Thus we can see, that although the Wolfenstein amplitudes A and C derived from the different NN potentials under study exhibit differences for large off-shell momenta, the off-shell region which is sampled in NA elastic scattering calculations is restricted to an area close to the on-shell value and thus does not probe those far off-shell regions where the larger differences occur.

## V. SUMMARY AND CONCLUSION

In this paper we addressed the question if nucleon-nucleus elastic scattering observables are sensitive to different off-shell structures of NN transition amplitudes derived from realistic NN potentials. Our study is based on the recently developed potential models NijmI and NijmII by the Nijmegen group [1] and the charge dependent Bonn potential [2]. All three potentials models describe the Nijmegen NN data base with a  $\chi^2$  per datum =1.03. Thus the transition matrices derived from these models can be considered on-shell equivalent. The Wolfenstein amplitudes, which enter our NA calculations, show considerable differences for large off-shell momenta. However, these differences are not visible in the NA elastic scattering observables.

We calculated elastic scattering observables for proton scattering from  $^{16}\text{O}$ ,  $^{40}\text{Ca}$ , and  $^{208}\text{Pb}$  in the energy regime between 100 and 200 MeV projectile energy. Here we calculated the full-folding integral for the first order optical potential using the impulse approximation within the framework of the spectator expansion of multiple scattering theory. In addition to the NN t-matrices from the three above mentioned potential models our optical potentials employ a Dirac-Hartree model for the nuclear density matrix. Recoil and frame transformation factors are implemented in the calculation in their complete form. We find that the elastic scattering observables based on the three different potential models are almost identical. A very similar result has been obtained in Ref. [7]. This work employs different density matrices and is based on the Paris potential and inversion potentials which are constructed to be phase-shift equivalent to the Paris potential as well as to the experimentally extracted phase shifts.

In order to better understand our numerical results, we study the regions of the NN t-matrices, which are sampled in a calculation of NA elastic scattering observables within the off-shell  $t\rho$  or optimum factorized approximation to the full-folding optical potential. In this approximation the off-shell character of the optical potential is solely determined by the off-shell NN t-matrix. This feature allows us to determine, which region of off-shell momenta for a fixed energy slice of the NN t-matrix enter the calculation. Our investigation of the rescattering term of the Lippmann-Schwinger equation shows, that the off-shell dependence of the optical potential is limited by the nuclear density, which in momentum space is a strongly peaked function for small momenta. It is well known that the heavier the nucleus becomes, the stronger is that forward peaking. This property of the nuclear density prevents far off-shell momenta of the NN t-matrix from entering the optical potential and thus the NA scattering observables. The coincidence of the calculations based on the different realistic



NN potentials strongly indicates that only off-shell momenta close to the on-shell value of the NN t-matrix are relevant for NA scattering. In this region the different potentials still give very similar results for the NN t-matrix.

Comparing our calculations of elastic scattering observables to experimental data, we still find some systematic inabilities of the first order full-folding optical potential to describe certain details for the NA scattering data in the considered energy regime. However, we find the limitations of the first order optical potential cannot be attributed to uncertainties associated with the off-shell behavior of the realistic NN t-matrices employed.

## ACKNOWLEDGMENTS

The authors want to thank W. Glöckle for many stimulating, helpful and critical discussion during this project.

This work was performed in part under the auspices of the U. S. Department of Energy including contract No. DE-FG02-93ER40756 with Ohio University. One of us (D.H.) would like to thank the Deutsche Forschungsgemeinschaft for their support. We thank the Ohio Supercomputer Center (OSC) for the use of their facilities under Grant No. PHS206 as well as the National Energy Research Supercomputer Center (NERSC) for the use of their facilities under the FY1997 Massively Parallel Processing Access Program.

## REFERENCES

- [1] V.G.J. Stoks, R.A.M. Klomp, C.P.F. Terheggen, and J.J. de Swart, Phys. Rev. **C49**, 2950 (1994).
- [2] R. Machleidt, F. Sammarruca, Y. Song, Phys. Rev. **C53**, R1483 (1996).
- [3] R.B. Wiringa, V.G.J. Stoks, and R. Schiavilla, Phys. Rev. **C51**, 38 (1995).
- [4] D.J. Ernst, J.T. Londergan, G.A. Miller, and R.M. Thaler, Phys. Rev. **C16**, 537 (1977).
- [5] E.R. Siciliano and R.M. Thaler, Phys. Rev. **C16**, 1322 (1977).
- [6] C.R. Chinn, Ch. Elster, R.M. Thaler, and S.P. Weppner, Phys. Rev. **C52**, 1992 (1995).
- [7] H.F. Arellano, F.A. Brieva, M. Sander, H.V. von Geramb, Phys. Rev. **C54**, 2570 (1996).
- [8] H.F. Arellano, F.A. Brieva, and W.G. Love, Phys. Rev. **C52**, 301 (1995); H.F. Arellano, F.A. Brieva, and W.G. Love, Phys. Rev. **C41**, 2188 (1990).
- [9] R. Crespo, R.C. Johnson, and J.A. Tostevin, Phys. Rev. **C41**, 2257 (1990).
- [10] Ch. Elster, S.P. Weppner, and C.R. Chinn, Phys. Rev. **C56**, 2080 (1997).
- [11] Ch. Elster and S.P. Weppner, to appear in Phys. Rev. C, and <http://xxx.lanl.gov/ps/nucl-th/9708010>
- [12] S.P. Weppner, Ph.D. Thesis, Ohio University, August 1997.
- [13] C.J. Joachain, 'Quantum Collision Theory' (North-Holland Physics 1987) p. 387.
- [14] C.J. Horowitz and B.D. Serot, Nucl. Phys **A368**, 503 (1981).
- [15] C.R. Chinn, Ch. Elster, and R.M. Thaler, Phys. Rev. **C44**, 1569 (1991).
- [16] A. Picklesimer, P. C. Tandy, R. M. Thaler, and D. H. Wolfe, Phys. Rev. **C30**, 1861 (1984).
- [17] D.J. Ernst and G.A. Miller, Phys. Rev. **C21**, 1472 (1980); D.L. Weiss and D.J. Ernst, Phys. Rev. **C26**, 605 (1982); D.J. Ernst, G.A. Miller, and D.L. Weiss, Phys. Rev. **C27**, 2733 (1983).
- [18] E.J. Stephenson, in 'Antinucleon- & Nucleon-Nucleus Interactions' Telluride, Co. 1985, pp 299, ed. by G. Walker et al. (Plenum Press, NY, 1985).
- [19] H.O. Meyer, P. Schwandt, G.L. Mooke, P.P. Singh, Phys. Rev. **C23**, 616 (1981); H.O. Meyer, P. Schwandt, W.W. Jacobs, J.R. Hall, Phys. Rev. **C27**, 459 (1983).
- [20] A. Nadasen, P. Schwandt, P.P. Singh, W.W. Jacobs, A.D. Bacher, P.T. Debevec, M.D. Kaitchuck, J.T. Meek, Phys. Rev. **C23**, 1023 (1981); P. Schwandt, H.O. Meyer, W.W. Jacobs, A.D. Bacher, S.E. Vigdor, M.D. Kaitchuck, T.R. Donoghue, Phys. Rev. **C26**, 55 (1982).
- [21] J. Kelly et al. Phys. Rev. Let. **45**, 2012 (1980) ; K. Amos et al., Nucl. Phys. **A413**, 255 (1984).

## FIGURES

FIG. 1. The angular distribution of the differential cross-section ( $\frac{d\sigma}{d\Omega}$ ), analyzing power ( $A_y$ ) and spin rotation function ( $Q$ ) are shown for elastic proton scattering from  $^{16}\text{O}$  at 200 MeV laboratory energy. The solid line represents the calculation performed with a first-order full-folding optical potential based on the DH density [14] and the CD-Bonn model [2]. The dashed line uses the NijmI model instead, the dash-dotted line the NijmII model [1]. The data are taken from Ref. [18].

FIG. 2. Same as Fig. 1, except that the target nucleus is  $^{40}\text{Ca}$ . The data are taken from Ref. [19].

FIG. 3. Same as Fig. 1, except that the target nucleus is  $^{208}\text{Pb}$ . The data are taken from Ref. [19].

FIG. 4. Same as Fig. 2, except that the projectile energy is 160 MeV. The data are taken from Ref. [20].

FIG. 5. Same as Fig. 1, except that the projectile energy is 135 MeV. The data are taken from Ref. [21].

FIG. 6. The real part of the function  $B(k_0, k_0, \theta, E)$  as defined in Eq. (4.4) for neutron scattering from  $^{16}\text{O}$  at 200 MeV laboratory energy. The solid line represents the full calculation, the dashed line, which coincides with the solid line, represents the calculation with an upper limit  $k_{max}$  in the k-integration of  $k_{max} = k_0 + 1.0 \text{ fm}^{-1}$ , while the dot-dashed line represents a calculation using  $k_{max} = k_0 + 0.5 \text{ fm}^{-1}$ .

FIG. 7. Same as Fig.6 that the nucleus is  $^{90}\text{Zr}$ . The solid line represents the full calculation, the dashed line, which coincides with the solid line, represents the calculation with an upper limit  $k_{max}$  in the k-integration of  $k_{max} = k_0 + 1.0 \text{ fm}^{-1}$ , while the dot-dashed line represents a calculation using  $k_{max} = k_0 + 0.5 \text{ fm}^{-1}$ . For the dotted line  $k_{max} = k_0 + 0.125 \text{ fm}^{-1}$  was used.

FIG. 8. The real part of the function  $B'(k_0, k_0, \theta, E)$  as defined in Eq. (4.5) for  $^{16}\text{O}$  at 200 MeV laboratory energy. The solid line represents the full calculation. The dash-dotted line represents the calculation with an upper limit  $k_{max}$  in the k-integration of  $k_{max} = k_0 + 1.5 \text{ fm}^{-1}$ , while the dashed line represents a calculation using  $k_{max} = k_0 + 1.0 \text{ fm}^{-1}$ . The values for  $\text{Re } B'$  are given in arbitrary units.

FIG. 9. The Wolfenstein amplitude  $\text{Re } A(k'_{NN}, k_{NN}, E_0)$  for np scattering at 200 MeV obtained from the NijmI potential [1]. The angle between  $\mathbf{k}_{NN}$  and  $\mathbf{k}'_{NN}$  is chosen to be zero. The contour lines represent steps of  $0.2 \text{ MeVfm}^3$ . The ‘skew box’ represents the region of momenta, which is accessed by a calculation of the NA scattering observables as described in the text.

FIG. 10. The difference of the Wolfenstein amplitudes  $Re A(k'_{NN}, k_{NN}, E_0)$  obtained by subtraction the amplitude obtained from the CD-Bonn potential [2] from the one obtained from the NijmI potential [1]. The angle between  $\mathbf{k}_{NN}$  and  $\mathbf{k}'_{NN}$  is chosen to be zero. The contour lines represent steps of  $0.2 \text{ MeVfm}^3$ .

FIG. 11. Same as Fig. 10, except that here the real part of the Wolfenstein amplitude  $A$  obtained from the NijmII potential is subtracted from the one obtained from the NijmI potential.

Fig.1

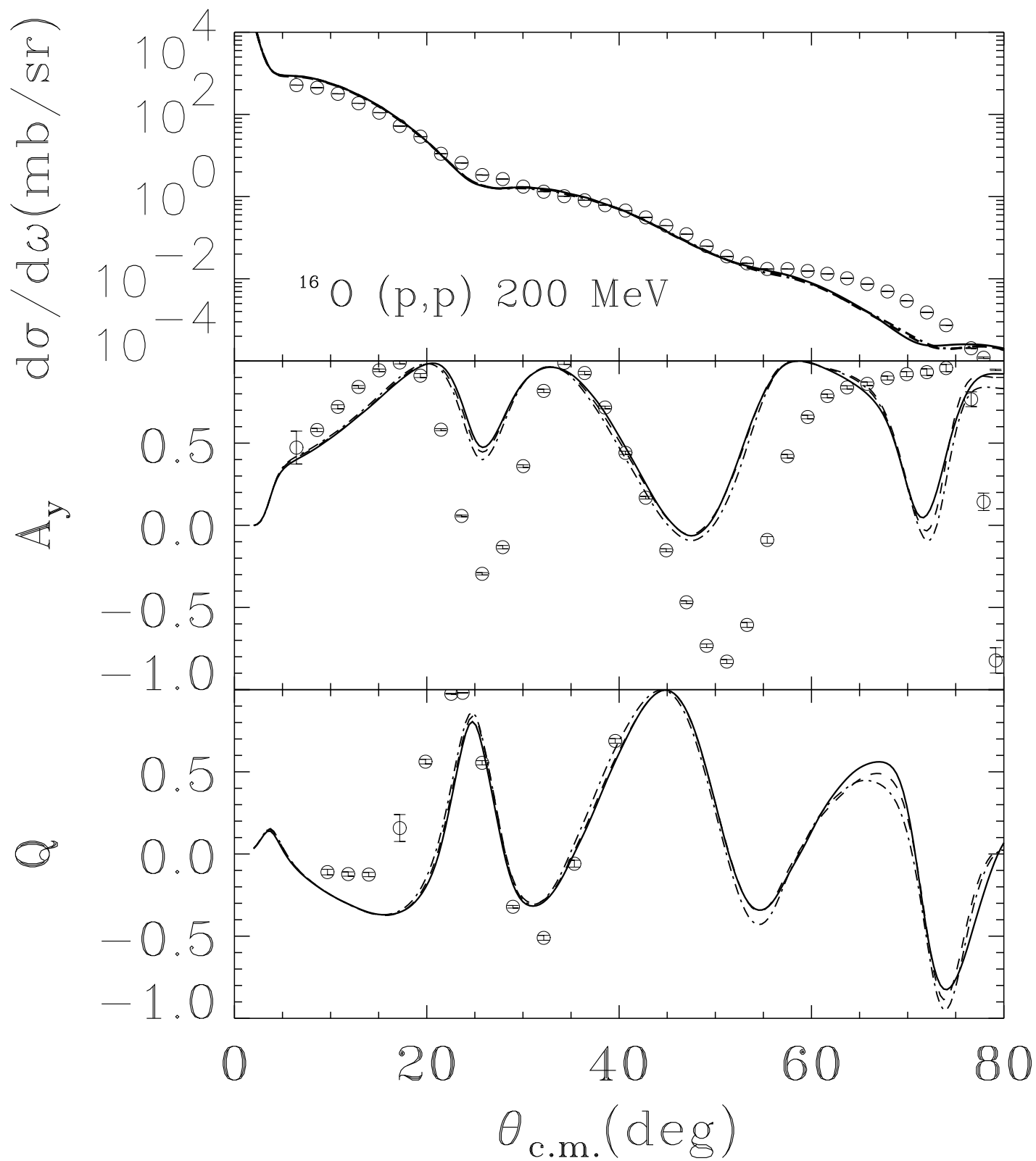


Fig.2

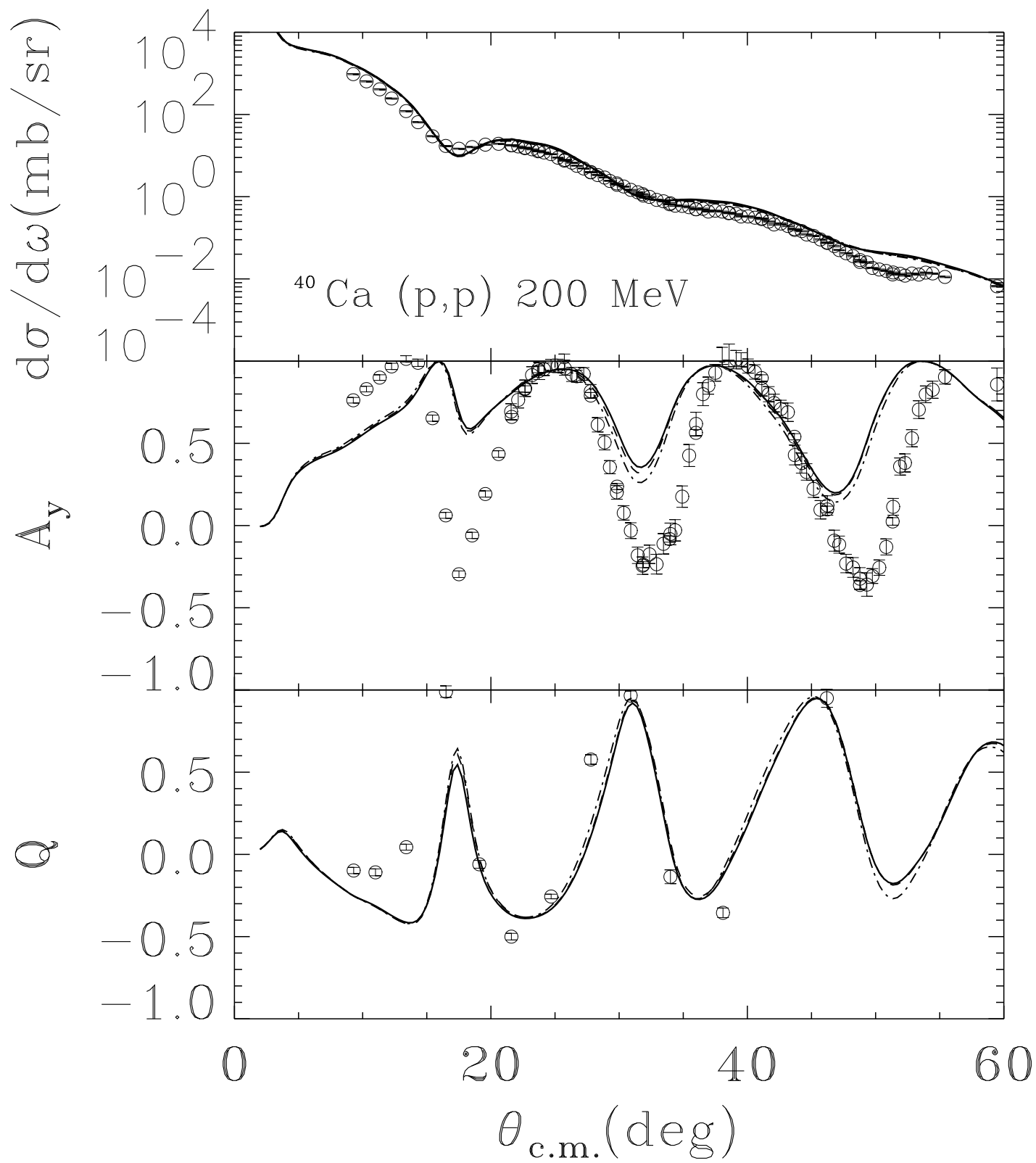


Fig.3

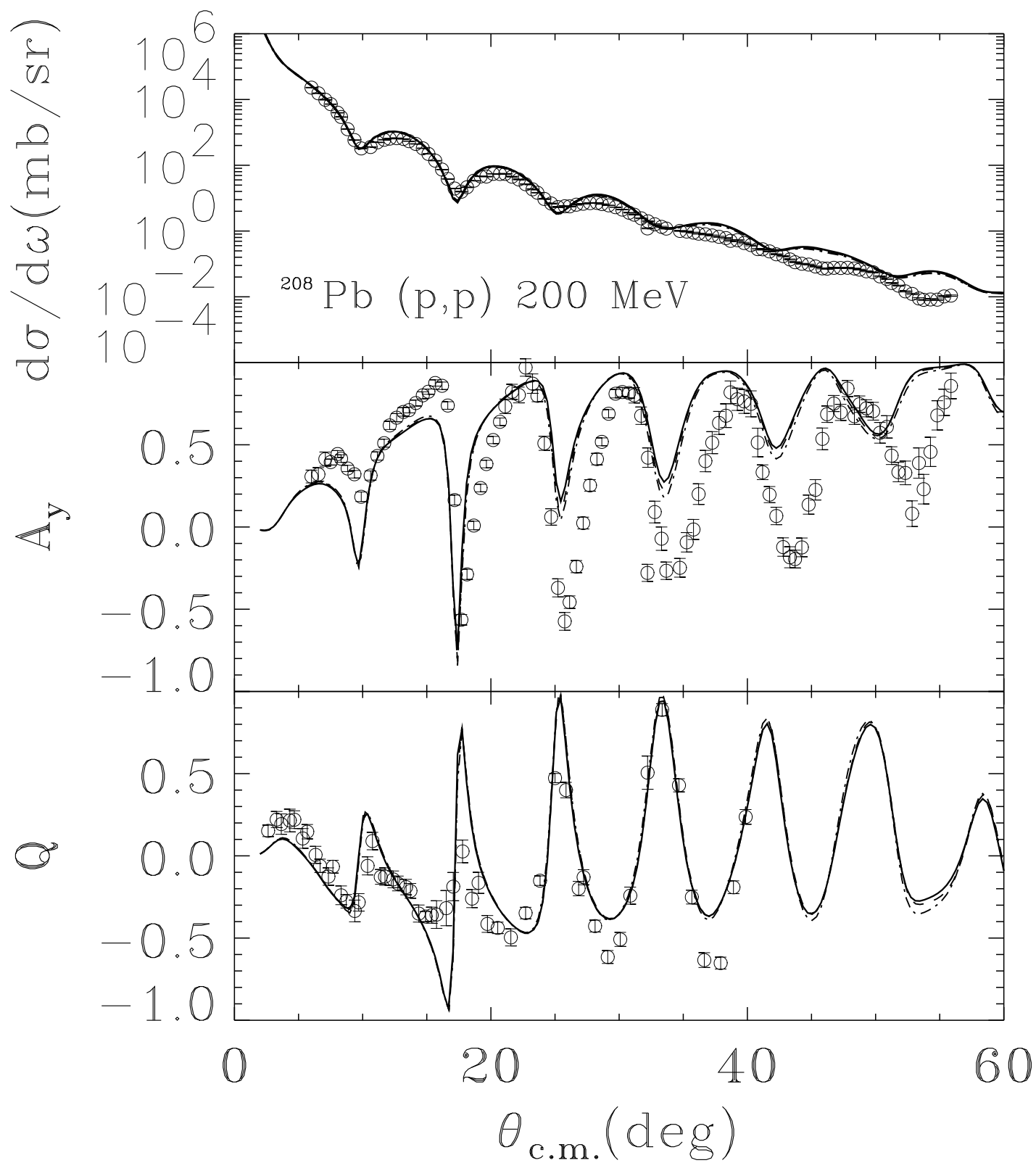


Fig.4

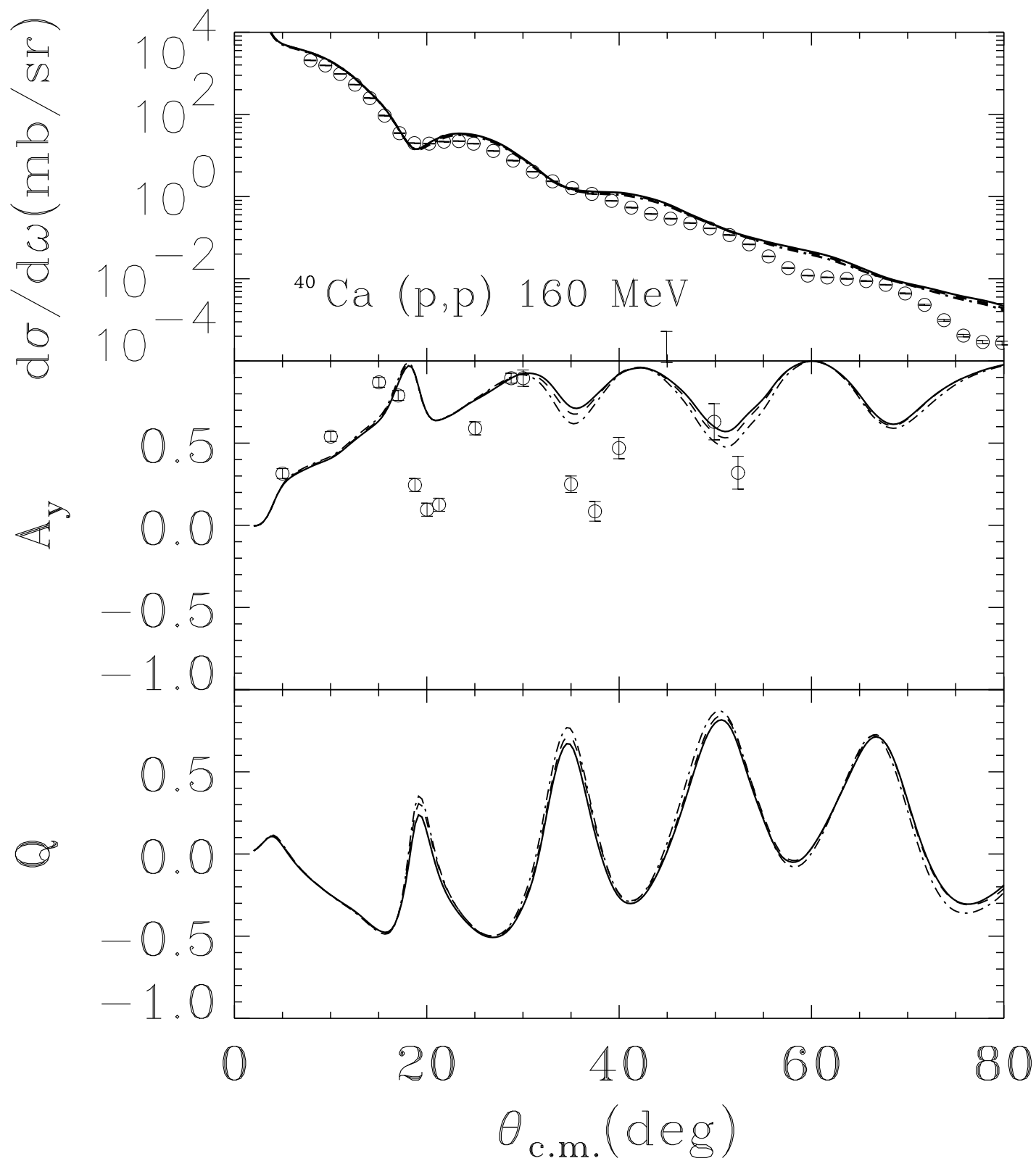




Fig.5

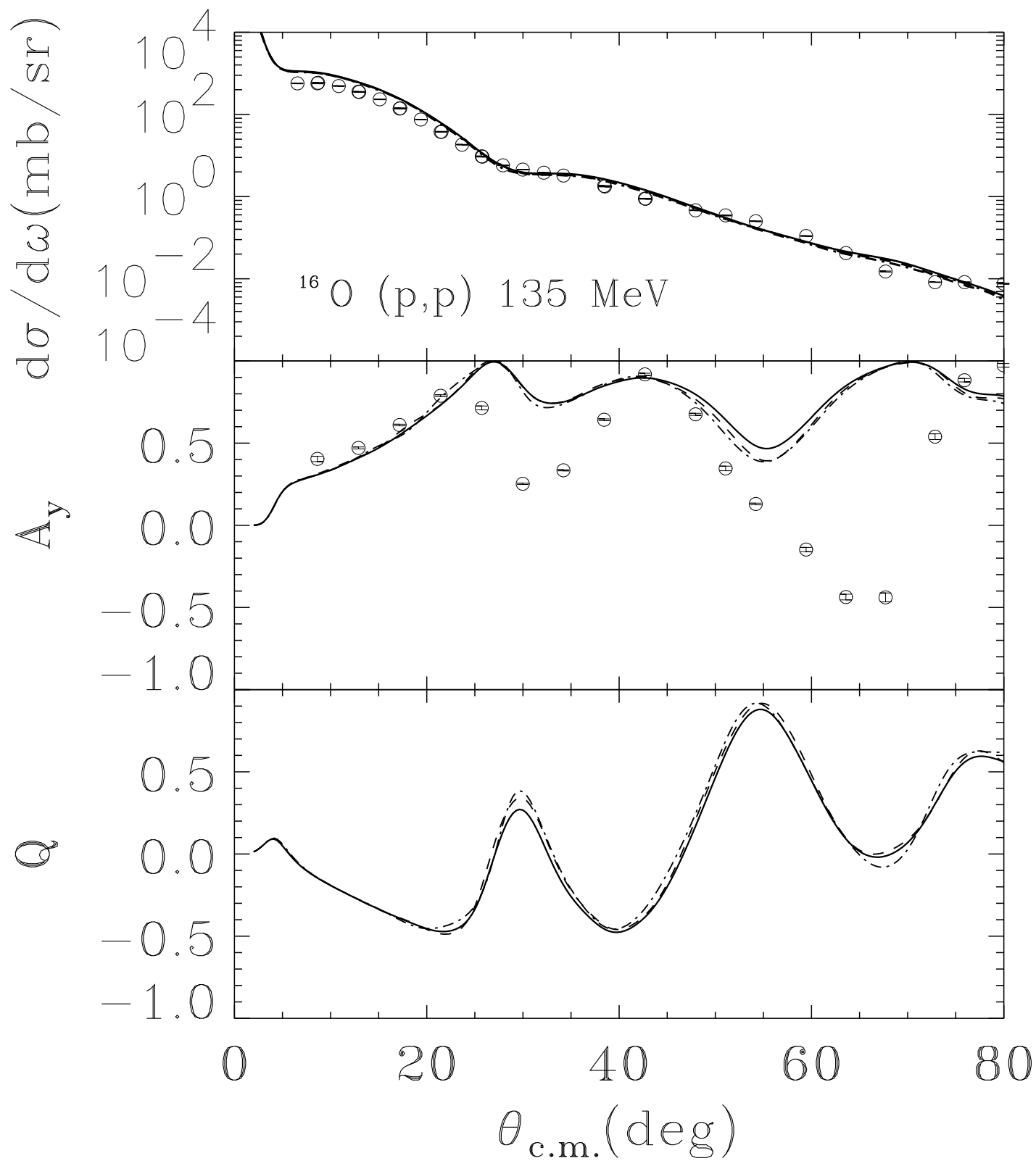


Fig. 6

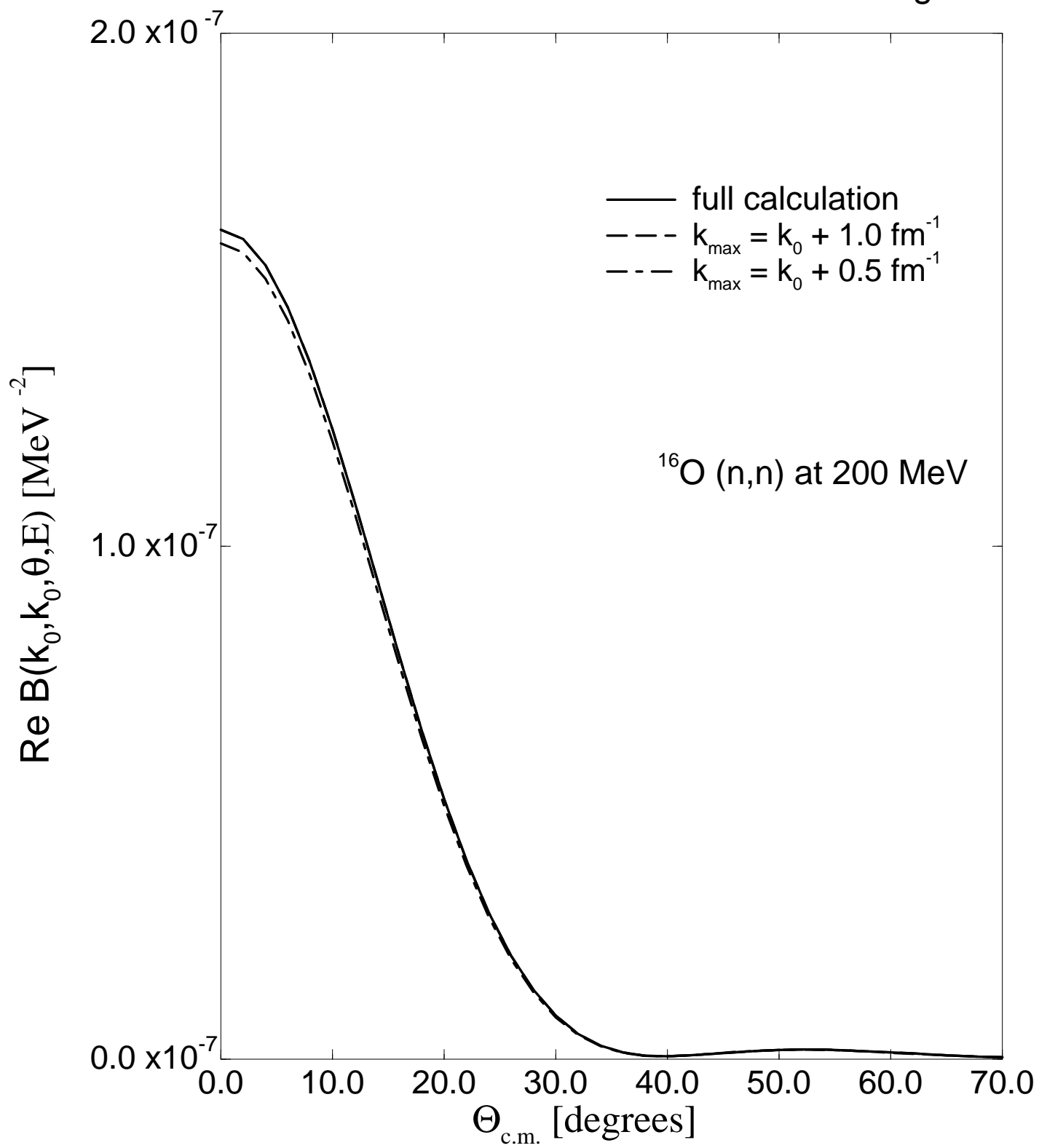


Fig. 7

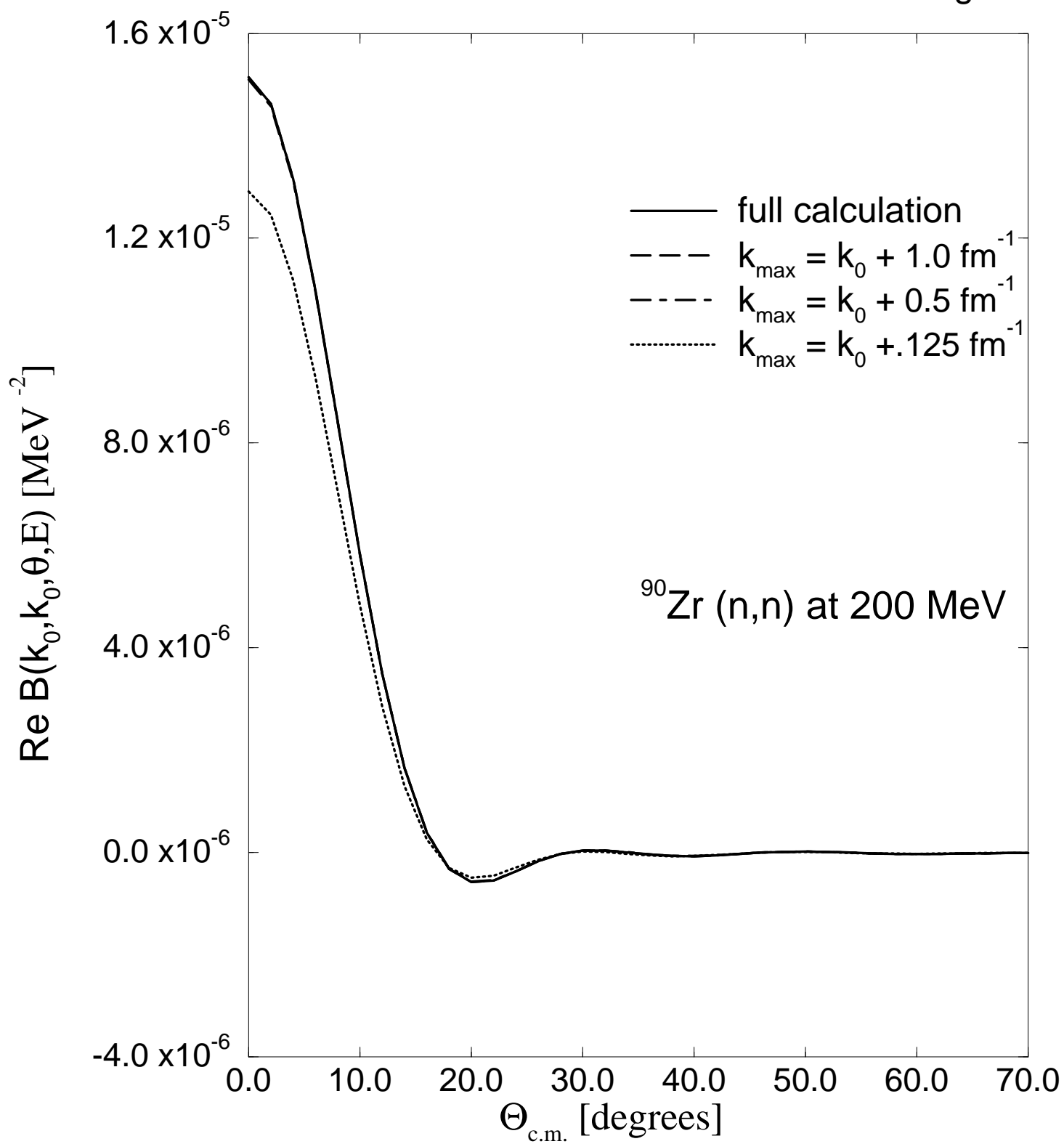


Fig. 8

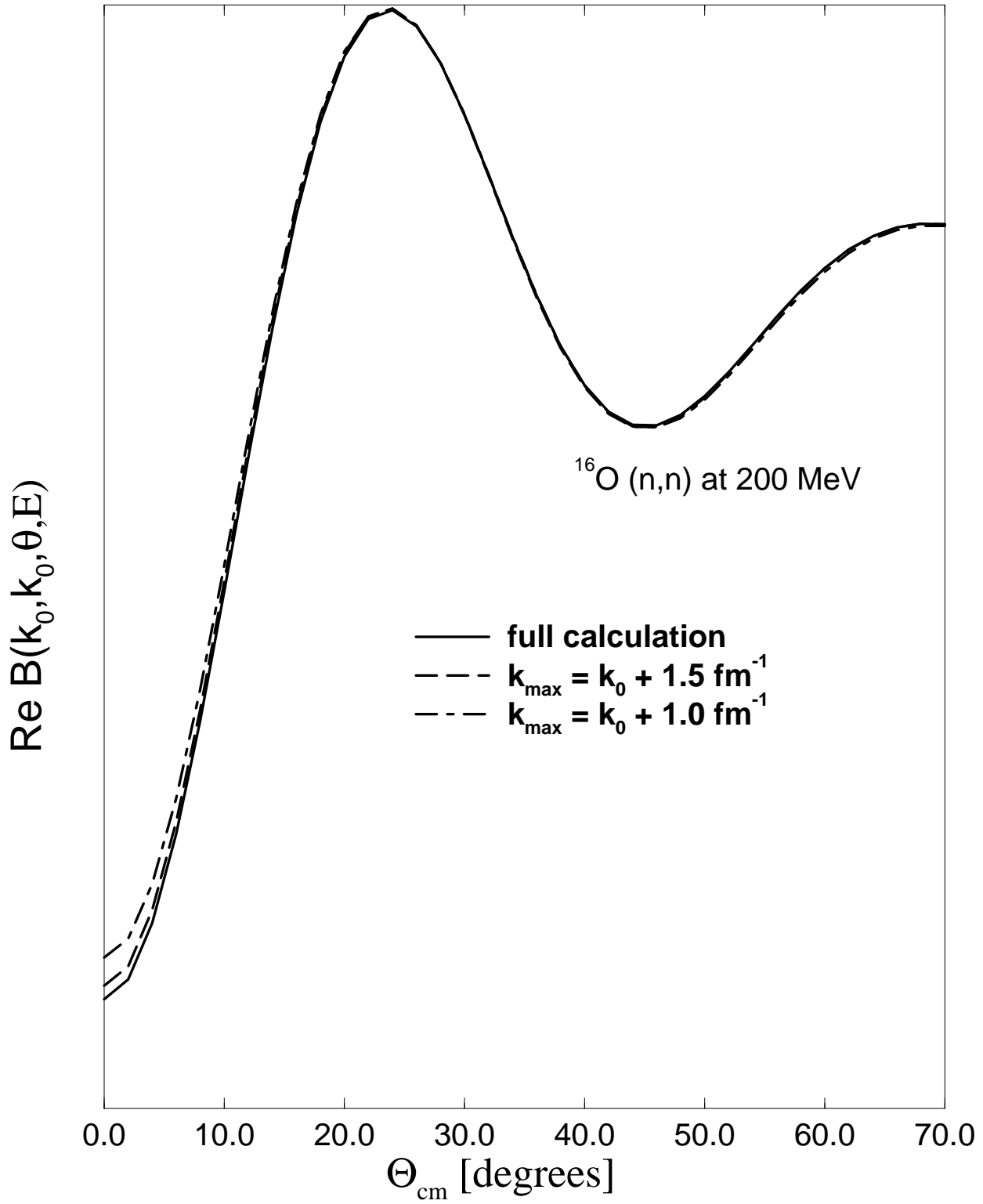


Fig.9

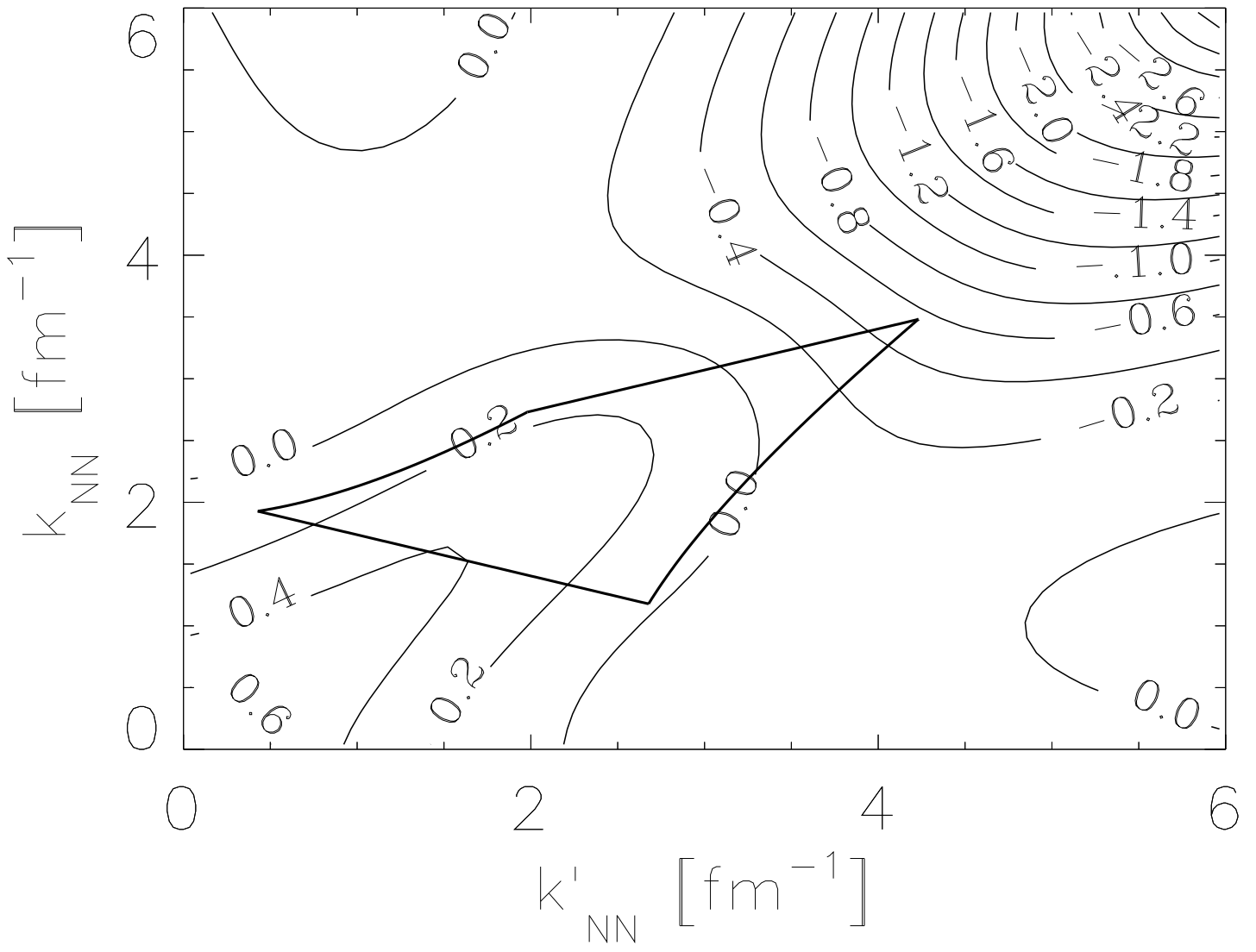


Fig.10

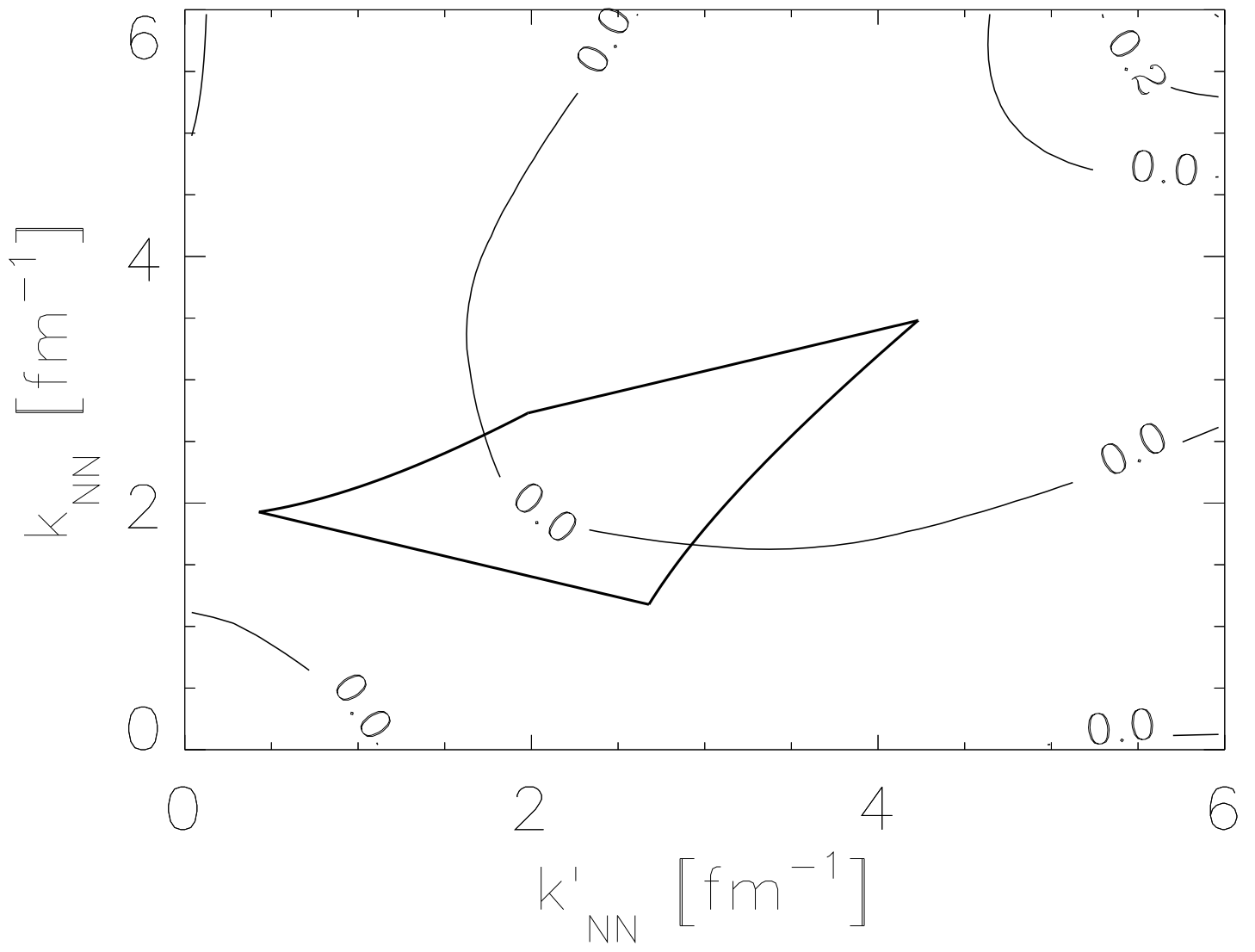


Fig.11

